NASA/TM–2012-104606, Vol. 31

Technical Report Series on Global Modeling and Data Assimilation, Volume 31

*Max J. Suarez, Editor*

# Global Surface Ocean Carbon Estimates in a Model Forced by MERRA

*Watson W. Gregg, Nancy W. Casey, and Cécile S. Rousseaux*

National Aeronautics and
Space Administration

**Goddard Space Flight Center**
Greenbelt, Maryland 20771

**September 2012**

# NASA STI Program ... in Profile

Since its founding, NASA has been dedicated to the advancement of aeronautics and space science. The NASA scientific and technical information (STI) program plays a key part in helping NASA maintain this important role.

The NASA STI program operates under the auspices of the Agency Chief Information Officer. It collects, organizes, provides for archiving, and disseminates NASA's STI. The NASA STI program provides access to the NASA Aeronautics and Space Database and its public interface, the NASA Technical Report Server, thus providing one of the largest collections of aeronautical and space science STI in the world. Results are published in both non-NASA channels and by NASA in the NASA STI Report Series, which includes the following report types:

- TECHNICAL PUBLICATION. Reports of completed research or a major significant phase of research that present the results of NASA Programs and include extensive data or theoretical analysis. Includes compilations of significant scientific and technical data and information deemed to be of continuing reference value. NASA counterpart of peer-reviewed formal professional papers but has less stringent limitations on manuscript length and extent of graphic presentations.

- TECHNICAL MEMORANDUM. Scientific and technical findings that are preliminary or of specialized interest, e.g., quick release reports, working papers, and bibliographies that contain minimal annotation. Does not contain extensive analysis.

- CONTRACTOR REPORT. Scientific and technical findings by NASA-sponsored contractors and grantees.

- CONFERENCE PUBLICATION. Collected papers from scientific and technical conferences, symposia, seminars, or other meetings sponsored or co-sponsored by NASA.

- SPECIAL PUBLICATION. Scientific, technical, or historical information from NASA programs, projects, and missions, often concerned with subjects having substantial public interest.

- TECHNICAL TRANSLATION. English-language translations of foreign scientific and technical material pertinent to NASA's mission.

Specialized services also include organizing and publishing research results, distributing specialized research announcements and feeds, providing help desk and personal search support, and enabling data exchange services. For more information about the NASA STI program, see the following:

- Access the NASA STI program home page at http://www.sti.nasa.gov

- E-mail your question via the Internet to help@sti.nasa.gov

- Fax your question to the NASA STI Help Desk at 443-757-5803

- Phone the NASA STI Help Desk at 443-757-5802

- Write to:

  NASA STI Help Desk
  NASA Center for AeroSpace Information
  7115 Standard Drive
  Hanover, MD 21076-1320

NASA/TM–2012-104606, Vol. 31

Technical Report Series on Global Modeling and Data Assimilation, Volume 31

## Global Surface Ocean Carbon Estimates in a Model Forced by MERRA

*Watson W. Gregg*
*NASA Goddard Space Flight Center, Greenbelt, Maryland*

*Nancey W. Casey*
*Science Systems and Applications, Inc., Lanham, Maryland*

*Cécile S. Rousseaux*
*Universities Space Research Association (GESTAR)*
*NASA Goddard Space Flight Center, Greenbelt, Maryland*

# Abstract

MERRA reanalysis products were used to force an established ocean biogeochemical model to estimate surface carbon inventories and fluxes in the global oceans. The results were compared to public archives of in situ carbon data and estimates. The model exhibited skill for ocean dissolved inorganic carbon (DIC), partial pressure of ocean $CO_2$ ($pCO_2$) and air-sea fluxes ($FCO_2$). The MERRA-forced model produced global mean differences of 0.02% (approximately 0.3 µM) for DIC, -0.3% (about -1.2 µatm; model lower) for $pCO_2$, and -2.3% (-0.003 mol C m$^{-2}$ y$^{-1}$) for $FCO_2$ compared to in situ estimates. Basin-scale distributions were significantly correlated with observations for all three variables (r=0.97, 0.76, and 0.73, P<0.05, respectively for DIC, $pCO_2$, and $FCO_2$). All major oceanographic basins were represented as sources to the atmosphere or sinks in agreement with in situ estimates. However, there were substantial basin-scale and local departures.

# Table of Contents

# List of Figures

# 1    Introduction

The oceans play a critical role in the global carbon cycle.  More than 90% of the active non-geological carbon pool resides in the oceans (Kaufman, 1998).  Estimates of global primary production suggest that the oceans contribute about half (Field et al., 1998).  One quarter (Le Quéré et al., 2010) of the carbon emitted by anthropogenic sources is thought to be sequestered in the oceans.   Understanding the role of the ocean in the global carbon cycle is a driving question in modern Earth science.  It requires foremost a geographically-distributed, well-maintained observational capability.  We are fortunate that such a capability exists or is in development, and that global data sets of ocean carbon inventories (Key et al., 2004), partial pressure of $CO_2$ (Takahashi et al., 2006; 2009) and atmospheric exchange (Takahashi et al., 2006; 2009) are publicly available.

 The Modern-Era Retrospective analysis for Research and Applications (MERRA) project represents a next generation of reanalysis products.  Utilizing data from NASA Earth observing satellites, MERRA is intended to improve upon the widely recognized set of existing reanalysis products, primarily by including a more realistic representation of the hydrological cycle (Rienecker et al., 2011).   A comprehensive approach using advanced data assimilation methodologies and modern Earth remote sensing observations, along with state of the art atmospheric and hydrological models, MERRA is expected to fully support climate-related modeling efforts.

Here we use MERRA reanalysis products to force a global ocean biogeochemical model.  We seek to 1) simulate the distributions and fluxes of carbon components in the global oceans with an explicit, prognostic description of the carbon cycle and 2) evaluate the realism of the model results.  The simulation is accomplished using an established three-dimensional model of the global oceans containing prognostic representations of biological and chemical constituents involved in the ocean carbon cycle.   Evaluation is achieved through comparison with observations of surface carbon inventories and fluxes.

# 2    Methods

## 2.1   Global Three-Dimensional Circulation Model

Global ocean carbon dynamics are simulated by the NASA Ocean Biogeochemical Model (NOBM; Figure 1). A complete description of the model can be found in Appendix 1. It is a three-dimensional representation of coupled circulation/ biogeochemical/radiative processes in the global oceans (Gregg et al., 2003; Gregg and Casey, 2007). It spans the domain from $-84^{o}$ to $72^{o}$ latitude in increments of $1.25^{o}$ longitude by $2/3^{o}$ latitude, including only open ocean areas, where bottom depth>200m. The biogeochemical processes model contains 4 phytoplankton groups, 4 nutrient groups, a single herbivore group, and 3 detrital pools (Figure 2). The phytoplankton groups differ in maximum growth rates, sinking rates, nutrient requirements, and optical properties. The 4 nutrients are nitrate, regenerated ammonium, silica to regulate diatom growth, and iron. Three detrital pools provide for storage of organic material, sinking, and eventual remineralization.

NASA Ocean Biogeochemical Model (NOBM)
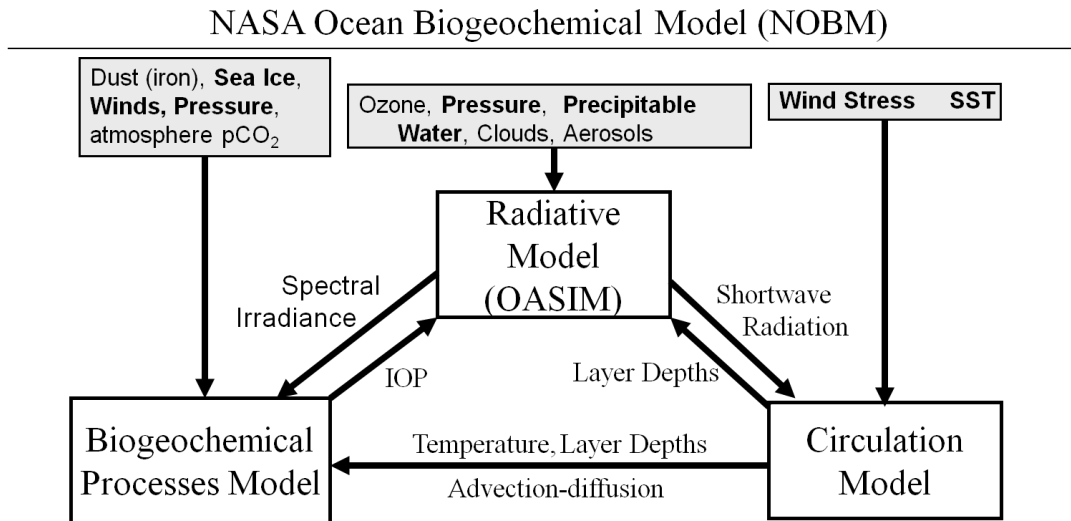


Figure 1. Interactions among the main components of NOBM, nominal outputs, and forcing fields. IOP indicates inherent optical properties. Forcing variables are shown in the gray boxes. MERRA forcing variables are in bold. Surface pressure and precipitable water effects on surface irradiance play a small role in the inorganic carbon results and are ignored in this effort.

Carbon cycling involves dissolved organic carbon (DOC) and dissolved inorganic carbon (DIC; Figure 2). DOC has sources from phytoplankton, herbivores, and carbon detritus, and a sink to DIC. DIC has sources from phytoplankton, herbivores, carbon detritus, and DOC, and communicates with the atmosphere, which can be either a source or sink. The ecosystem sink for DIC is phytoplankton, through photosynthesis. This represents the biological pump portion of the carbon dynamics. The solubility pump portion is represented by the interactions among temperature, alkalinity (parameterized as a function of salinity), silica, and phosphate (parameterized as a function of nitrate). The alkalinity/salinity parameterization utilizes the spatial variability of salinity in the model adjusted to mean alkalinity

$$TA = \underline{TA}\ S/\underline{S}$$

8

where TA is total alkalinity and S is salinity. The underscore represents global mean values. TA is specified as 2310 μE kg$^{-1}$ (Ocean Model Intercomparison Project (OCMIP; www.ipsl.jussieu.fr/OCMIP) and S as 34.8 PSU (global model mean). Since the model contains nitrate but not phosphate, we adjust nitrate by multiplying by 0.1. This is derived from the global mean ratio of nitrate to phosphate from the National Oceanographic Data Center (Conkright et al., 2002) for their top three standard levels. The calculations for the solubility pump follow the standards set by the Ocean Model Intercomparison Project (reference above). We employ a locally-developed lookup table valid over modern ranges of DIC, salinity, temperature, and nutrients for computational efficiency, at no cost to accuracy. Air-sea $CO_2$ exchange uses the Wanninkhof (1992) formulation, as is common in global and regional ocean carbon models (e.g., McKinley et al., 2006).
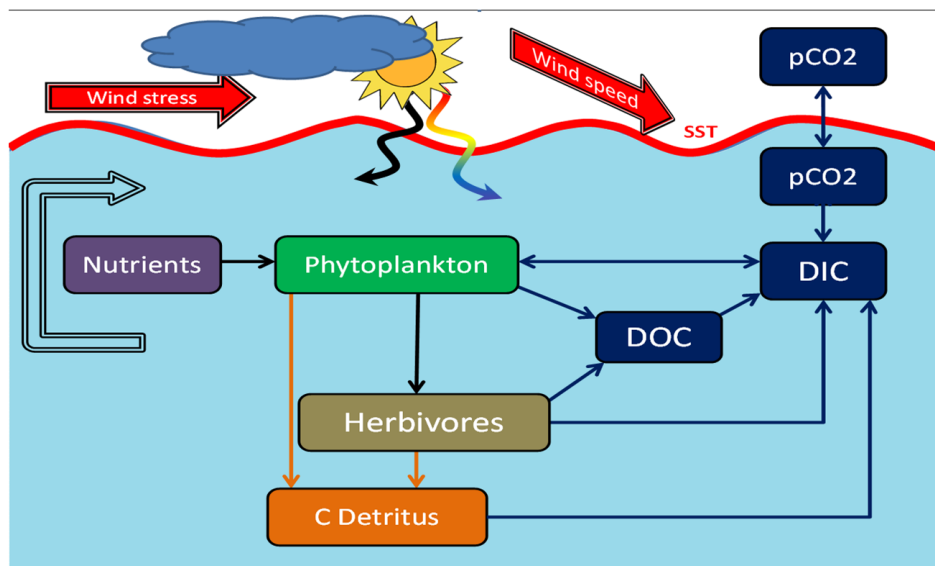


Figure 2. Pathways and interactions among the components of the biogeochemical processes model, illustrating the interactions with the carbon cycle, comprising dissolved inorganic carbon (DIC), dissolved organic carbon and exchanges with the atmosphere as a function of the ocean and atmosphere partial pressures of CO2 (pCO2). The biological pump is represented by phytoplankton, herbivores, nutrients, and detritus.

We acknowledge that the parameterization of alkalinity using salinity is a simplification. However, the relationship in the modern oceans is robust, especially in tropical and subtropical oceans (Millero et al., 1998; Key et al., 2004; Lee et al., 2006) and has been recommended for international carbon model intercomparison efforts (www.ipsl.jussieu.fr/OCMIP). Furthermore, the salinity-parameterization of alkalinity used in the model compares favorably globally and over major oceanographic basins with in situ data sets for the modern oceans (Figure 3). The basins are shown in Figure 4.

NOBM undergoes spin-up for 200 years under climatological forcing from MERRA. Initial conditions for DIC are derived from the Global Data Analysis Project (GLODAP; Key et al., 2004). We average DIC over oceanographic basins and depth and use these mean values for initial conditions. DOC initial conditions are set to 0 μM. Other initial conditions are described in Gregg and Casey (2007). The first ten years of the run show a net pCO$_2$ difference ΔpCO$_2$

(year 10-year 1) of -0.982 µatm, at the first hundred years the 10-year $\Delta pCO_2$ (year 100-year 91) is 0.413 µatm, and at 200 years, the 10-year $\Delta pCO_2$ (year 200-year 191) is 0.102 µatm.
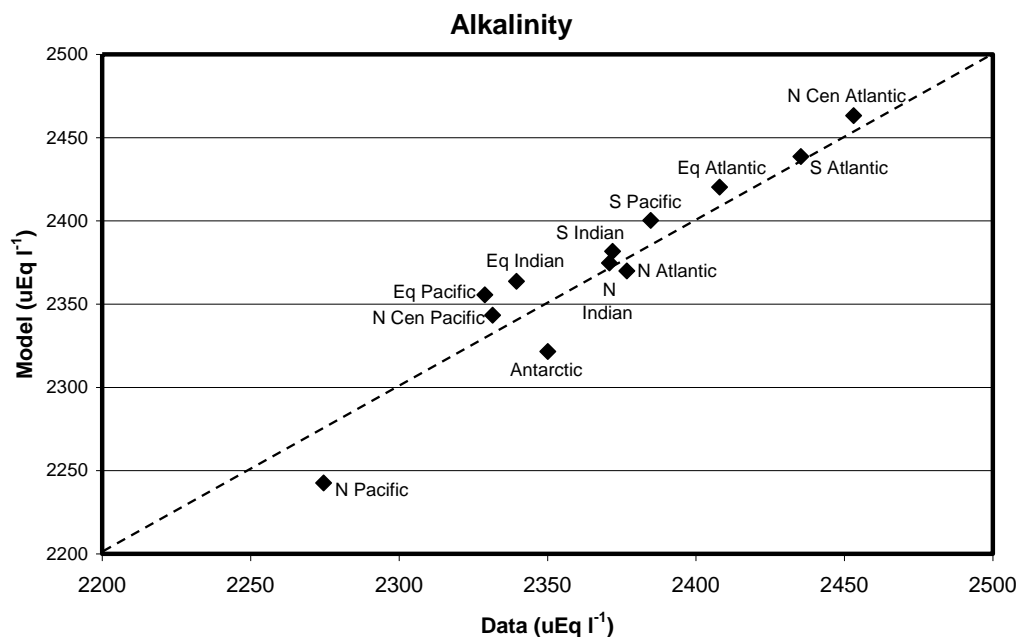


Figure 3.  Annual surface alkalinity distributions and statistics from the model and data.   The model-data basin correlation is statistically significant at P<0.05, as indicated by an asterisk.
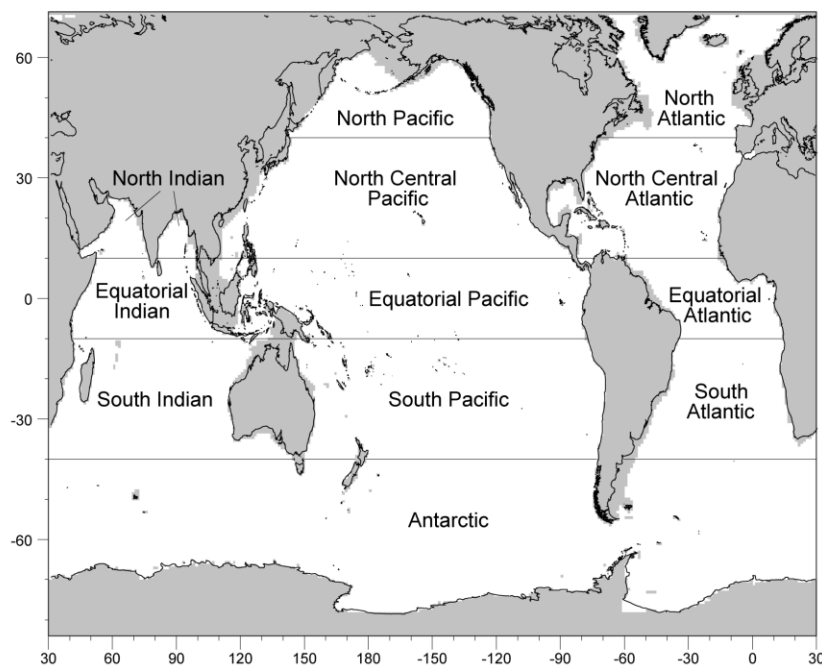


Figure 4.  Delineation of the 12 major oceanographic basins.

## 2.2   Data Sets

### 2.2.1   Forcing Data Sets

Forcing data sets are shown in Figure 1.  Monthly climatologies are used in all cases.  All except soil dust (iron), ozone, clouds, and atmospheric $CO_2$ are obtained from MERRA products. Ozone is from the Total Ozone Mapping Spectrometer and Ozone Monitoring Instrument, and soil dust deposition is from Ginoux et al. (2001).  Cloud data (cover and liquid water path) are obtained from the International Satellite Cloud Climatology Project.  Atmospheric $CO_2$ is taken from the Lamont-Doherty Earth Observatory (LDEO) data set (Takahashi et al., 2009), using a mean over the entire range of observations of 358.7 µatm.   Although the ocean $pCO_2$ observations are nominally normalized to the year 2000 (Takahashi et al., 2009), we keep the mean atmospheric value from the data to help represent the spatial variability at the time of measurement.  Our emphasis is to understand how the simulated surface carbon components compare with in situ data sets, so using atmospheric values from these datasets facilitates the comparison.

*Comparison Data Sets*

The main outputs of interest in this effort are dissolved inorganic carbon (DIC), partial pressure of $CO_2$ ($pCO_2$), and the flux of $CO_2$ ($FCO_2$, notation following Arrigo et al., 2010; Doney et al., 2009), representing the exchange of carbon between the atmosphere and ocean (positive is defined upward, indicating a source to the atmosphere).  DIC data sets are obtained from GLODAP (Key et al., 2004), which are mapped on a $1^o$ horizontal grid with 33 standard depth levels (http://cdiac.ornl.gov/oceans/glodap/).  $pCO_2$ and $FCO_2$ data sets are mapped on a $5^o$ longitude by $4^o$ latitude horizontal grid and are surface only.  They are obtained from the Lamont-Doherty Earth Observatory (LDEO)

(http://cdiac.ornl.gov/oceans/LDEO_Underway_Database/index.html; Takahashi et al., 2009).

### 2.2.2   Methodological Approach

The global model NOBM is forced with the MERRA variables shown in bold in Figure 1.  The model is spun up for 199 years using monthly climatologies of MERRA forcing.  In the $200^{th}$ year of simulation, model results of surface ocean carbon are compared graphically and statistically with climatological in situ data sets and estimates from GLODAP (DIC) and LDEO ($pCO_2$ and $FCO_2$).  Results are evaluated globally and regionally in 12 major oceanographic basins (Figure 4).  Statistical comparisons include global and basin differences between model and data global and regional means, expressed as percent, and correlation analysis.  Our emphasis is on large scale results, so our correlation analysis is performed across the basins (N=12, with 10 degrees of freedom).  All analyses here are performed for annual mean results, and the data sets are converted to the NOBM spatial grid prior to comparison.

# 3    Results

Surface DIC from NOBM compares favorably with in situ data (Figure 5). There is substantial geographical similarity, and basins follow similar patterns. The global difference is 0.02%, representing $\Delta DIC=0.3\mu M$, with a correlation across basins of 0.97, which is statistically significant at P<0.05. The most notable differences are the tropical upwelling regions. Upwelling in the Equatorial Pacific is not apparent in the in situ data, while it is prominent in the model. The in situ data show a depression in DIC in the Equatorial Atlantic upwelling region, which is in contrast to an increase seen in the model. The basin mean, however, is in agreement (Figure 5). The model also has modestly lower DIC in most of the Antarctic. The largest basin difference is 1.2% in the Equatorial Indian and Pacific ($\Delta DIC=24.5\mu M$ and $\Delta DIC=23.3\mu M$, respectively). The remaining basin differences are <1%.
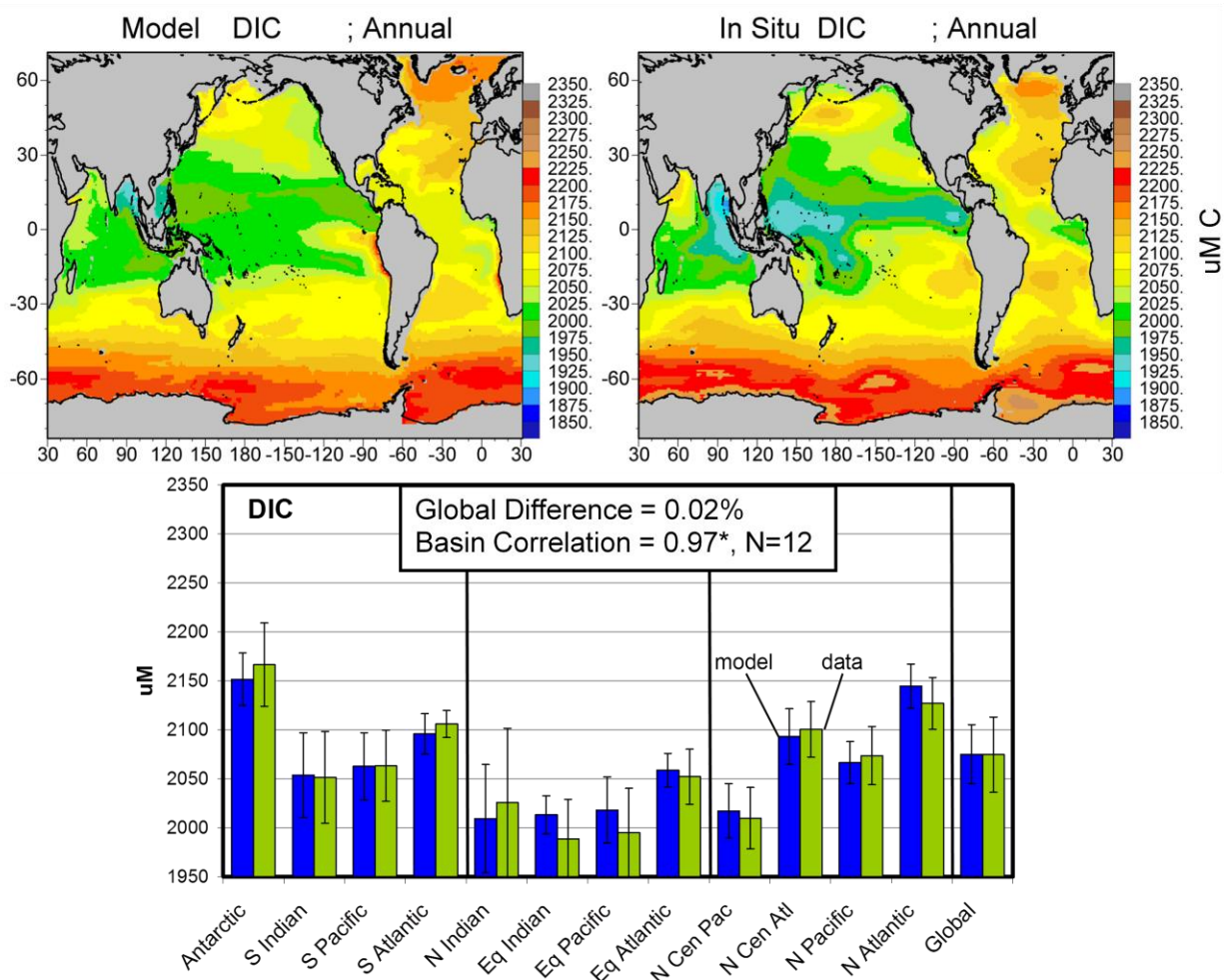


Figure 5. Annual surface dissolved inorganic carbon (DIC) distributions and statistics from the model (blue) and data (green). The model-data basin correlation is statistically significant at P<0.05, as indicated by an asterisk. Southern, tropical, and northern basins are delineated on the bar graph. Error bars indicate the standard deviation.

There is also considerable similarity between the model and in situ data in global $pCO_2$ distributions (Figure 6). The global difference is -0.3% (model lower), which is a difference of -

1.2 µatm. The correlation across basins is statistically significant with r = 0.76. The model $pCO_2$ distributions are in general agreement in the tropical Pacific upwelling, in contrast with DIC, and there is no depression in the tropical Atlantic in the $pCO_2$ data. There is an east-west departure in the North and Equatorial Indian basins between the model and data, with lower values in the model in the west, and higher values in the east. There is much more spatial variability in the model, as seen in the maps and also the standard deviations (Figure 6). The largest basin difference is -8.9% in the South Atlantic ($\Delta pCO_2$=-32.3µatm) followed by the Equatorial Indian at 4.3% ($\Delta pCO_2$=16.1µatm). The remaining basin differences are <4%. The largest local discrepancies are in the eastern South Pacific and Atlantic, where the model exhibits two regions of depressed $pCO_2$ relative to the data, representing about a 35% difference.
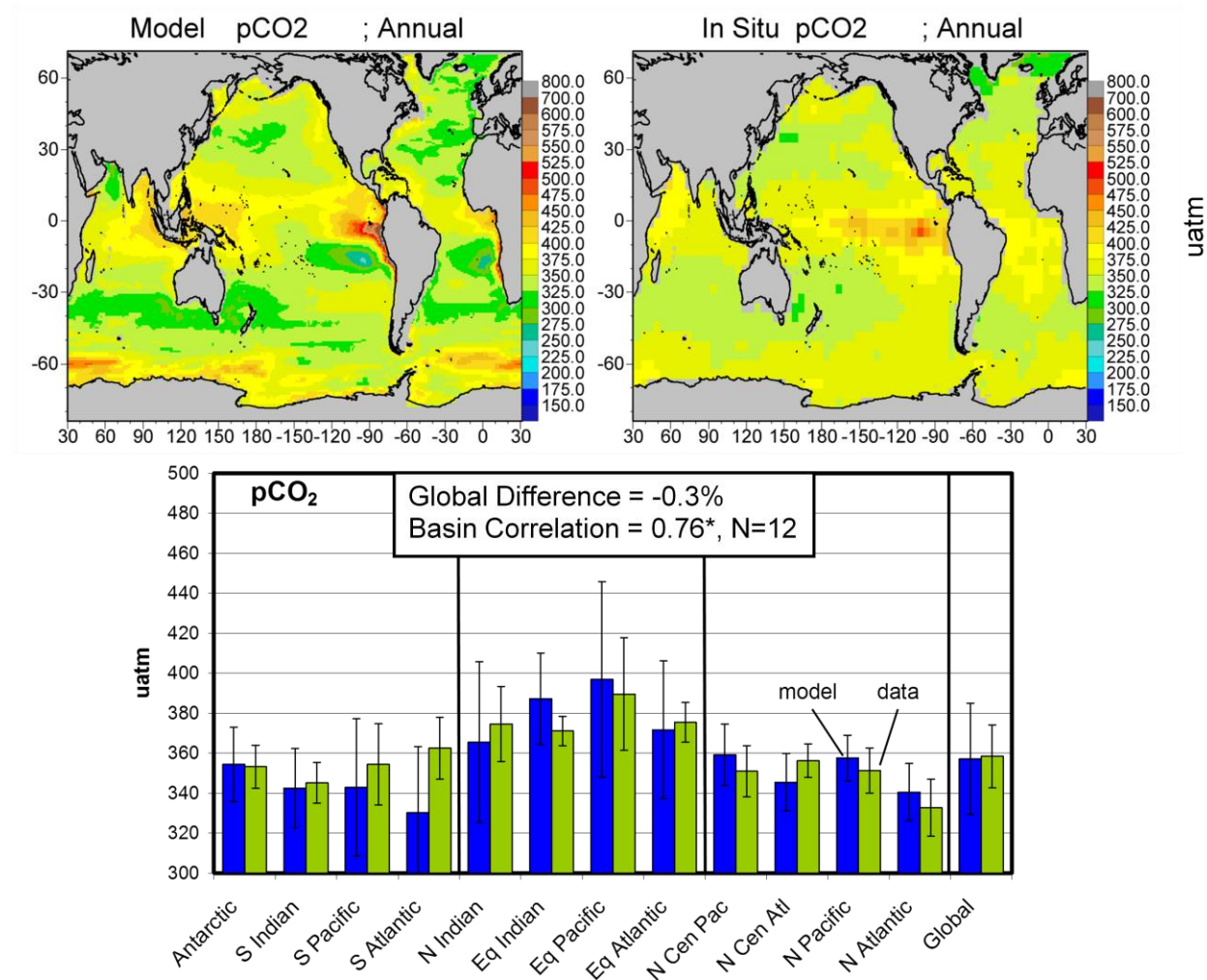


Figure 6. Annual partial pressure $CO_2$ ($pCO_2$; uatm) distributions and statistics from the model (blue) and data (green). The model-data basin correlation is statistically significant at P<0.05, as indicated by an asterisk. Southern, tropical, and northern basins are delineated on the bar graph. Error bars indicate the standard deviation.

There are many areas of agreement in the flux of $CO_2$ ($FCO_2$) between the model and in situ estimates, but there are also many areas of disagreement and they are more pronounced than with DIC and $pCO_2$ (Figure 7). The global difference is -2.3%, representing $\Delta FCO_2$=0.003 mol C m$^{-2}$

y$^{-1}$.  Like DIC and pCO$_2$, the basin correlation is statistically significant (r=0.73, P<0.05).  The sign of the flux (source or sink) is the same for model and in situ estimates in all the basins, but there are large differences in some basins, such as the South Atlantic and Pacific, North Indian, Equatorial Atlantic, and North Pacific.
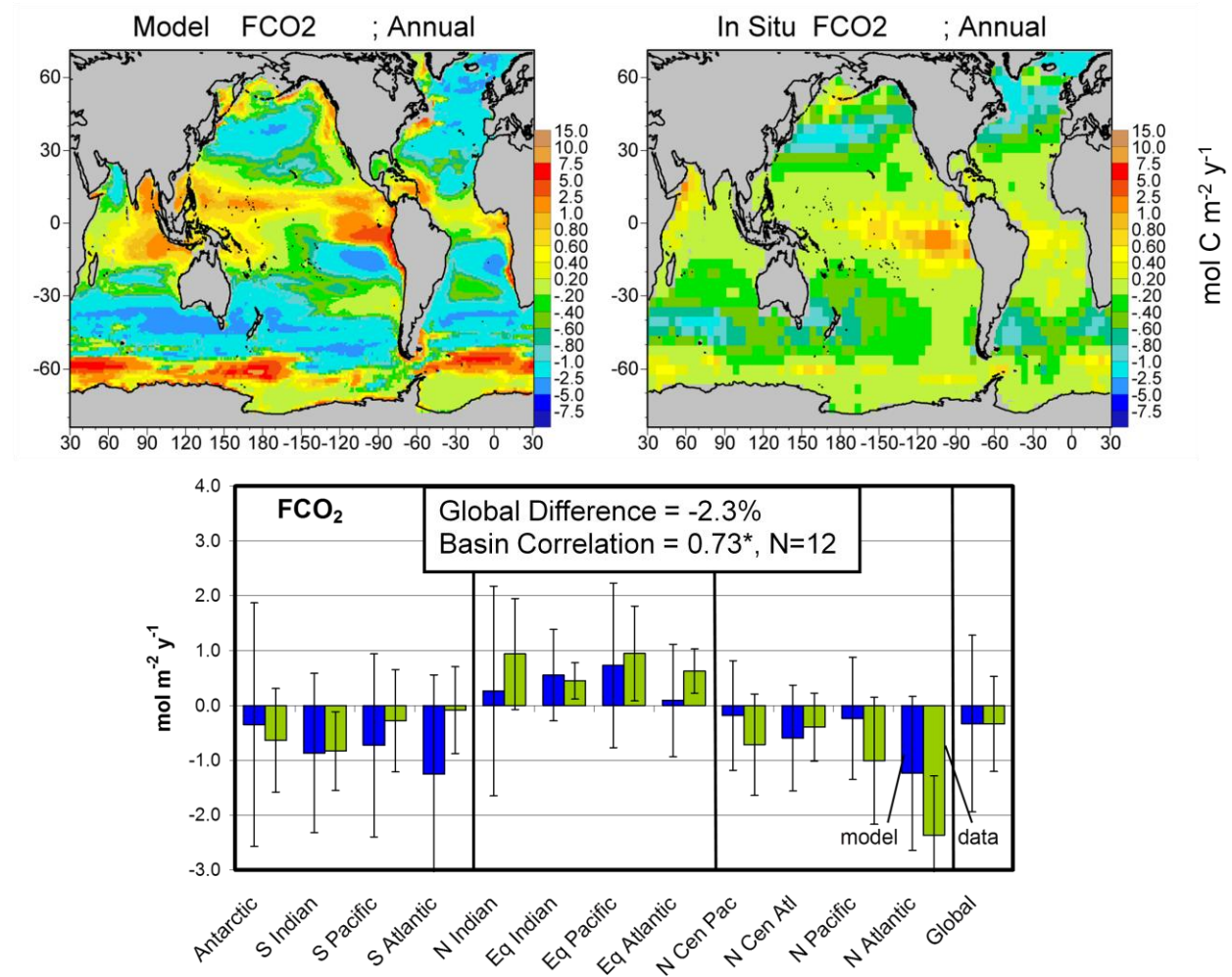


Figure 7. Annual CO$_2$ flux (FCO$_2$) distributions and statistics from the model (blue) and data (green). The model-data basin correlation is  statistically significant at P<0.05, as indicated by the asterisk.  Southern, tropical, and northern basins are delineated on the bar graph.  A positive flux indicates a source to the atmosphere.  Error bars indicate the standard deviation.

   There is much greater spatial variability in the model than the in situ estimates of air-sea flux, as indicated in the maps and the standard deviations of the basin means (Figure 7).  Locally, there are major sinks represented in the model in the northeastern portions of the South Pacific and Atlantic that do not appear in the data estimates (Figure 7).  The Antarctic exhibits regions of strong sources that are also not apparent in the data.  The location of sources and sinks in the North and Equatorial Indian basins are switched in the model from the data, where the model shows a sink in the west and a source in the east, while the data show the reverse pattern.

# 4    Discussion

The MERRA-forced biogeochemical model (NOBM) produces global estimates of DIC, $pCO_2$, and $FCO_2$ to within a few percent of corresponding in situ data sets and estimates. The global mean difference is 0.02%, -0.3%, and -2.3% respectively for DIC, $pCO_2$, and $FCO_2$, and all show statistically positive correlation with data ($P<0.05$) across the 12 major oceanographic basins. Our emphasis here is global and basin scales representations of ocean carbon surface inventories and fluxes, as appropriate for a global model, and the results suggest that NOBM, forced by MERRA atmospheric and oceanic variables, possesses skill for simulating ocean carbon quantities at these large spatial scales.

We acknowledge that the agreement for DIC is perhaps not surprising, since it was used for initial conditions. But it is noteworthy that the model is able to hold these large scale distributions over 200 years, and also exhibit substantial agreement with smaller scale distributions (Figure 5). We note that, in contrast to $pCO_2$ and $FCO_2$, the spatial variability of model DIC, as represented by the standard deviation, is similar to in situ data on global and basin scales.

The global scale agreement of carbon estimates from the model with in situ sources is encouraging, and is the main emphasis here, but it is notable that at smaller scales the agreement is not as good. Basin and local discrepancies increase as one evaluates the carbon from DIC to $pCO_2$ to $FCO_2$. The increase in basin and local scales from $pCO_2$ to $FCO_2$ is a reflection of the fact that small discrepancies between model and data in DIC and $pCO_2$ can produce important differences in $FCO_2$. Thus $FCO_2$ is sensitive to small errors in DIC and $pCO_2$, and it can be a challenge to represent this well in models, especially at smaller scales and using a global model.

We note that use of atmospheric $pCO_2$ for year 2000 only modestly changes the results shown here. Specifically, the global mean difference is 0.3%, 2.2%, and 7.8% respectively for DIC, $pCO_2$, and $FCO_2$, and again all show statistically positive correlation with data ($P<0.05$) across the 12 major oceanographic basins. The differences represent a stronger flux into the oceans as expected from the higher atmospheric $pCO_2$ (368.6 instead of 358.7 µatm).

# 5    References

Agawin, N.S.R., C.M. Duarte, and S. Agusti, 1998. Growth and abundance of *Synechococcus* sp. in a Mediterranean Bay: Seasonality and relationship with temperature. Marine Ecology Progress Series 170: 45-53.

Agawin, N.S.R., C.M. Duarte, and S. Agusti, 2000. Nutrient and temperature control of the contribution of picoplankton to phytoplankton biomass and production. Limnology and Oceanography 45: 591-600.

Ahn, Y.-H., A. Bricaud, and A. Morel, 1992. Light backscattering efficiency and related properties of some phytoplankters. Deep-Sea Research 39: 1835-1855.

Archer, D.E. and K. Johnson, 2000. A model of the iron cycle in the ocean. Global Biogeochemical Cycles 14: 269-279.

Arrigo, K.R., Pabi, S., van Dijken, G.L., and Maslowski, W., 2010. Air-sea flux of CO2 in the Arctic Ocean, 1998–2003. Journal of Geophysical Research Vol. 115, G04024, doi:10.1029/2009JG001224

Aumont, O., S. Belviso, and P. Monfray, 2002. Dimethylsulfoniopropionate (DMSP) and dimethylsulfide (DMS) sea surface distributions simulated from a global three-dimensional ocean carbon cycle model. Journal of Geophysical Research 107: doi: 10.1029/1999JC000111.

Barlow, R.G. and R.S. Alberte, 1985. Photosynthetic characteristics of phycoerythrin-containing marine *Synechococcus spp.* Marine Biology 86: 63-74.

Bates, S.S. and T. Platt, 1984. Fluorescence induction as a measure of photosynthetic capacity in marine phytoplankton: response of *Thalassiosira pseudonana* (Bacillariophyceae) and *Dunaliella tertiolecta* (Chlorophyceae). Marine Ecology Progress Series 18: 67-77.

Ben-Amotz, A. and A. Gilboa, 1980. Cryptopreservation of marine unicellular algae. I. A survey of algae with regard to size, culture age, photosynthetic activity and chlorophyll – to - cell ratio. Marine Ecology Progress Series 2: 157-161.

Brand, L.E., W.G. Sunda, and R.R.L. Guillard, 1983. Limitation of marine phytoplankton reproductive rates by zinc, manganese, and iron. Limnology and Oceanography 28: 1182-1198.

Brand, L.E., W.G. Sunda, and R.R.L. Guillard, 1986. Reduction of marine phytoplankton reproduction rates by copper and cadmium. Journal of Experimental Marine Biology and Ecology 96: 225-250.

Bricaud, A., Morel, A., and L. Prieur, 1983. Optical efficiency factors of some phytoplankton. Limnology and Oceanography 28: 816-832.

Bricaud, A. and A. Morel, 1986. Light attenuation and scattering by phytoplanktonic cells: a theoretical modeling. Applied Optics 25: 571-580.

Bricaud, A., A.-L. Bedhomme, and A. Morel, 1988. Optical properties of diverse phytoplanktonic species: experimental results and theoretical interpretation. Journal of Plankton Research 10: 851-873.

Carpenter, E.J. and K. Romans, 1991. Major role of the cyanobacterium *Trichodesmium* in nutrient cycling in the North Atlantic Ocean. Science 254: 1356-1358.

Conkright, M.E., S. Levitus and T.P. Boyer, 1994. World Ocean Atlas, Volume 1: Nutrients, NOAA Atlas NESDIS 1, 150 pp.

Conkright, M.E., Garcia, H.E., O'Brien, T.D., Locarnini, R.A., Boyer, T.P., Stephens, C., Antonov, J.I., 2002. World Ocean Atlas 2001, Volume 4: Nutrients. S. Levitus, Ed., NOAA Atlas NESDIS 52, U.S. Government Printing Office, Wash., D.C., 392 pp.

Csanady, G.T., 1986. Mass transfer to and from small particles in the sea, Limnology and Oceanography 31: 237-248.

Doney, S.C., K. Lindsay, K. Caldeira, J.-M. Campin, H. Drange, J.-C. Dutay, M. Follows, Y. Gao, A. Gnanadeskin, N. Gruber, A. Ishida, F. Joos, G. Madec, E. Maier- Reimer, J.C. Marshall, R.J. Matear, P. Monfray, A. Mouchet, R. Najjar, J.C. Orr, G.-K. Plattner, J. Sarmiento, R. Schlitzer, R. Slater, I.J. Totterdell, M.-F. Weirig, Y. Yamanaka, and A. Yool, 2004. Evaluating global ocean carbon models: The importance of realistic physics. Global Biogeochemical Cycles 18: 10.1029/2003GB002150.

Doney, S.C. and 7 others, 2009. Mechanisms governing interannual variability in upper-ocean inorganic carbon system and air–seaCO2 fluxes: Physical climate and atmospheric dust. Deep-Sea Research II 56: 640–655.

Dubinsky, Z. and T. Berman, 1986. Light utilization efficiencies of phytoplankton in Lake Kinneret (Sea of Galilee). Limnology and Oceanography 21: 226-230.

Dutay, J.-C., J.L. Bullister, S.C. Doney, J.C. Orr, R. Najjar, K. Caldeira, J.-M. Campin, H. Drange, M. Follows, Y. Gao, N. Gruber, M.W. Hecht, A. Ishida, F. Joos, K. Lindsay, G. Madec, E. Maier-Reimer, J.C. Marshall, R.J. Matear, P. Monfray, A. Mouchet, G.-K. Plattner, J. Sarmiento, R. Schlitzer, R. Slater, I.J. Totterdell, M.-F. Weirig, Y. Yamanaka, and A. Yool, 2002. Evaluation of ocean model ventilation with CFC-11: Comparison of 13 global ocean models. Ocean Modelling 4: 89-120.

Eppley, R.W., J.N. Rogers, and J.J. McCarthy, 1969. Half-saturation constants for uptake of nitrate and ammonium by marine phytoplankton. Limnology and Oceanography 14: 912-920.

Eppley, R.W., 1972. Temperature and phytoplankton growth in the sea. Fisheries Bulletin 70: 1063-1085.

Falkowski, .G., Z. Dubinsky, and K. Wyman, 1985. Growth-irradiance relationships in phytoplankton. Limnology and Oceanography 30: 311-321.

Field, C.B., M.J. Behrenfeld, J.T. Randerson, and P. Falkowski, 1998. Primary production of the biosphere: Integrating terrestrial and oceanic components. Science 281: 237-240.

Fritz, J.J. and W.M. Balch, 1996. A light-limited continuous culture study of *Emiliana huxleyi*: Determination of coccolith detachment and its relevance to cell sinking. Journal of Experimental Marine Biology and Ecology 207: 127-147.

Fung, I.Y., S.K. Meyn, I. Tegen, S.C. Doney, J.G. John, and J.K.B. Bishop, 2000. Iron supply and demand in the upper ocean. Global Biogeochemical Cycles 14: 281-295.

Furnas, M.J., 1991. Net in situ growth rates of phytoplankton in an oligotrophic, tropical shelf ecosystem. Limnology and Oceanography 36: 13-29.

Gavis, J., R.R.L. Guillard, and B.L. Woodward, 1981. Cupric ion activity and the growth of phytoplankton clones isolated from different marine environments. Journal of Marine Research 39: 315-333.

Ginoux, P., M. Chin, I. Tegen, J.M. Prospero, B. Holben, O. Dubovik, and S.-J. Lin, 2001. Sources and distributions of dust aerosols simulated with the GOCART model. Journal of Geophysical Research 106, 20255-20273.

Goldman, J.C. and P.M. Glibert, 1982. Comparative rapid ammonium uptake by four species of marine phytoplankton. Limnology and Oceanography 27: 814-827.

Gorgues, T., Aumont, O., and Rodgers, K.B., 2010. A mechanistic account of increasing seasonal variations in the rate of ocean uptake of anthropogenic carbon. Biogeosciences 7: 2581–2589.

Gregg, W.W. and K.L. Carder, 1990. A simple spectral solar irradiance model for cloudless maritime atmospheres. Limnology and Oceanography 35: 1657-1675.

Gregg, W.W. and J.J. Walsh, 1992. Simulation of the 1979 spring bloom in the Mid-Atlantic Bight: A coupled physical/biological/optical model. Journal of Geophysical Research 97: 5723-5743.

Gregg, W.W., 2002. A coupled ocean-atmosphere radiative model for global ocean biogeochemical models. NASA Global Modeling and Assimilation Series, M. Suarez, ed. NASA Technical Memorandum 2002-104606, Vol. 22, 33 pp. Available at GMAO website https://gmao.gsfc.nasa.gov/pubs/tm/archive/tm_2002.php.

Gregg, W.W., P. Ginoux, P.S. Schopf, and N.W. Casey, 2003. Phytoplankton and Iron: Validation of a global three-dimensional ocean biogeochemical model. Deep-Sea Research II 50: 3143-3169.

Gregg, W.W. and Casey, N.W., 2007.  Modeling coccolithophores in the global oceans. Deep-Sea Research II 54: 447-477.

Humphrey, G.F., 1979.  Photosynthetic characteristics of algae grown under constant illumination and light-dark regimes. Journal of Experimental Marine Biology and Ecology 40: 63-70.

Kaufman, Y.J.,, Herring, D.D., Ranson, K.J., and Collatz, G.J., 1998.  Earth observing system AM1 mission to Earth.  IEEE Transactions Geoscience and Remote Sensing 36: 1045-1055.

Key, R.M., A. Kozyr, C.L. Sabin, K. Lee, R. Wanninkhof, J.L. Bullister, R.A. Feely, F.J. Millero, C. Mordy, and T.-H. Peng, 2004.  A global ocean carbon climatology: Results from Global Data Analysis Project (GLODAP).  Global Biogeochemical Cycles 18: 10.1029/2004GB002247.

Kirk, J.T.O., 1980.  Spectral properties of natural waters: Contribution of the soluble and particulate fractions to light absorption in some inland waters of southeastern Australia. Australian Journal of Marine and Freshwater Research 31: 287-296.

Langdon, C., 1987.  On the causes of interspecific differences in the growth-irradiance relationship for phytoplankton. Part I. A comparative study of the growth-irradiance relationship of three marine phytoplankton species: *Skeletonema costatum, Olisthodiscus luteus*, and *Gonyaulax tamarensis.* Journal of Plankton Research 9: 459-482.

Lee, K., Tong, L.T., Millero, F.J., Sabine, C.L., Dickson, A.G., Goyet, C., Park, G.-H., Wanninkhof, R., Feely, R.A., and Key, R.M., 2006.  Global relationships of total alkalinity with salinity and temperature in surface waters of the world's oceans. Geophysical Research Letters, Vol. 33, L19605, doi:10.1029/2006GL027207.

Le Quéré, C., Takahashi, T., Buitenhuis, E.T., Rodenbeck, C., and Sutherland, S.C., 2010.  Impact of climate change and variability on the global oceanic sink of CO2.  Global Biogeochemical Cycles, Vol. 24, GB4007, doi:10.1029/2009GB003599.

McGillicuddy, D.J., J.J. McCarthy, and A.R. Robinson, 1995.  Coupled physical and biological modeling of the spring bloom  in the North Atlantic (I): Model formulation and one dimensional bloom processes.  Deep-Sea Research 42: 1313-1357.

McKinley, G.A., T. Takahashi,  E. Buitenhuis, F. Chai, J. R. Christian,S. C. Doney, M.-S. Jiang, K. Lindsay, J. K. Moore, C. Le Quéré, I. Lima, R. Murtugudde, L. Shi, and P. Wetzel. 2006.  North Pacific carbon cycle response to climate variability on seasonal to decadal timescales. Journal of Geophysical Research, Vol. 111, C07S06, doi:10.1029/2005JC003173.

Millero, F.J., Lee, K., Roche, M., 1998.  Distribution of alkalinity in the surface waters of the major oceans.  Marine Chemistry 60: 111-130.

Mitchell, B.G. and D.A. Kiefer, 1988.  Chlorophyll a specific absorption and fluorescence excitation spectra for light-limited phytoplankton. Deep-Sea Research 35: 639-663.

Moore, J.K., S.C. Doney, D.M. Glover, and I.Y. Fung, 2002.  Iron cycling and nutrient-limitation patterns in the surface waters of the world ocean.  Deep-Sea Research II 49: 463-507.

Morel, A. 1987.  Chlorophyll-specific scattering coefficient of phytoplankton. A simplified theoretical approach. Deep-Sea Research 34: 1093-1105.

Morel, A. and A. Bricaud, 1981.  Theoretical results concerning light absorption in a discrete medium, and application to specific absorption of phytoplankton.  Deep-Sea Research 28: 1375-1393.

Perry, M.J., M.C. Talbot, and R.S. Alberte, 1981.  Photoadaptation in marine phytoplankton: response of the photosynthetic unit. Marine Biology 62: 91-101.

Rienecker, M. M., M.J. Suarez, R. Gelaro, R. Todling, J. Bacmeister, E. Liu, M.G. Bosilovich, S.D. Schubert, L. Takacs, G.-K. Kim, S. Bloom, J. Chen, D. Collins, A. Conaty, A. da Silva, et al., 2011. MERRA - NASA's Modern-Era Retrospective Analysis for Research and Applications. *J. Climate*, 24, 3624-3648. doi: 10.1175/JCLI-D-11-00015.1.

Sakshaug, E. and K. Andresen, 1986. Effect of light regime upon growth rate and chemical composition of a clone of *Skeletonema costatum* from the Trondheimsfjord, Norway. Journal of Plankton Research 8: 619-637.

Sathyendranath, S., L. Lazzara, and L. Prieur, 1987. Variations in the spectral values of specific absorption of phytoplankton. Limnology and Oceanography 32: 403-415.

Schopf, P.S. and A. Loughe, 1995. A reduced gravity isopycnal ocean model: Hindcasts of El Nino. Monthly Weather Review 123: 2839-2863.

Subba Rao, D.V., 1981. Growth response of marine phytoplankton to selected concentrations of trace metals. Botanica marina 24: 369-379.

Sunda, W.G. and S.A. Huntsman, 1995. Iron uptake and growth limitation in oceanic and coastal Phytoplankton. Marine Chemistry 50: 189-206.

Takahashi, T., Sutherland, S.C., Feely, R.A., and Wanninkhof, R., 2006. Decadal change of the surface water pCO2 in the North Pacific: A synthesis of 35 years of observations. Journal of Geophysical Research 111, C07S05, doi:10.1029/2005JC003074.

Takahashi, T., and 30 others, 2009. Climatological mean and decadal change in surface ocean pCO2, and net sea–air CO2 flux over the global ocean. Deep-Sea Research II 56: 554-577.

Wanninkhof,R.,1992. Relationship between wind speed and gas exchange over the ocean. Journal of Geophysical Research 97(C5), 7373–7382.

Wyman, M. and P. Fay, 1986. Underwater light climate and the growth and pigmentation of planktonic blue-green algae (Cyanobacteria) I. The influence of light quantity. Proceedings of the Royal Society of London 227: 367-380.

# 6    Appendix A

## 6.1   NASA Ocean Biogeochemical Model-Equations

The governing equations of the model are

*Phytoplankton*

$$\frac{\partial}{\partial t}P_i = \boldsymbol{\nabla}\bullet(K\boldsymbol{\nabla}P_i) - \boldsymbol{\nabla}\bullet\boldsymbol{V}P_i - \frac{\partial}{\partial z}(w_s)_i\, P_i + [\mu_i - (\delta + \Omega)]P_i - \gamma H - \kappa P_i \tag{A1}$$

i = 1 => diatoms
i = 2 => chlorophytes
i = 3 => cyanobacteria
i = 4 => coccolithophores

*Nutrients*

$$\frac{\partial}{\partial t}N_N = \boldsymbol{\nabla}\bullet(K\boldsymbol{\nabla}N_N) - \boldsymbol{\nabla}\bullet\boldsymbol{V}N_N - b_N\left[\Sigma_i\, \mu_i P_i\right] + R\alpha_c D_c/(C{:}N) + \lambda_D D_c/(C{:}N) \tag{A2}$$

$$\frac{\partial}{\partial t}N_A = \boldsymbol{\nabla}\bullet(K\boldsymbol{\nabla}N_A) - \boldsymbol{\nabla}\bullet\boldsymbol{V}N_A - b_N\left[\Sigma_i\, \mu_i P_i\right] + b_N\varepsilon[\gamma H + n_2 H^2] \tag{A3}$$

$$\frac{\partial}{\partial t}N_S = \boldsymbol{\nabla}\bullet(K\boldsymbol{\nabla}N_S) - \boldsymbol{\nabla}\bullet\boldsymbol{V}N_S - b_S\, \mu_1 P_1 + R\alpha_S D_S \tag{A4}$$

$$\frac{\partial}{\partial t}N_F = \boldsymbol{\nabla}\bullet(K\boldsymbol{\nabla}N_F) - \boldsymbol{\nabla}\bullet\boldsymbol{V}N_F - b_F[\Sigma_i\, \mu_i P_i] + b_F\varepsilon[\gamma H + \eta_2 H^2] + R\alpha_F D_F + A_{Fe}/L - \theta N_F \tag{A5}$$

$N_N$= nitrate
$N_A$ = ammonium
$N_S$ = silica
$N_F$ = dissolved iron

*Herbivores*

$$\frac{\partial}{\partial t}H = \boldsymbol{\nabla}\bullet(K\boldsymbol{\nabla}H) - \boldsymbol{\nabla}\bullet\boldsymbol{V}H - (1 - \varepsilon)\gamma H - \eta_1 H - \eta_2 H^2 - \omega H - \Theta H \tag{A6}$$

*Detritus*

$$\frac{\partial}{\partial t}D_C = \boldsymbol{\nabla}\bullet(K\boldsymbol{\nabla}D_C) - \boldsymbol{\nabla}\bullet\boldsymbol{V}D_C - \frac{\partial}{\partial z}(w_d)_C D_C - R\alpha_N D_C + \Phi[\kappa\Sigma_i\, P_i + \eta_1 H] + \Phi(1 - \varepsilon)\eta_2 H^2 - \lambda_D D_C \tag{A7}$$

$$\frac{\partial}{\partial t}D_S = \boldsymbol{\nabla}\bullet(K\boldsymbol{\nabla}D_S) - \boldsymbol{\nabla}\bullet\boldsymbol{V}D_S - \frac{\partial}{\partial z}(w_d)_S D_S - R\alpha_S D_S + b_S[\kappa P_1 + \gamma H] \tag{A8}$$

$$\frac{\partial}{\partial t} D_F = \boldsymbol{\nabla} \bullet (K \boldsymbol{\nabla} D_F) - \boldsymbol{\nabla} \bullet \boldsymbol{V} D_F - \frac{\partial}{\partial z}(w_d)_F D_F - R\alpha_F D_F + b_F[\kappa \Sigma_i P_i + \eta_1 H] + b_F(1-\varepsilon)\eta_2 H^2$$
$$+ \theta N_F \tag{A9}$$

$D_C$ = carbon/nitrogen detritus
$D_S$ = silica detritus
$D_F$ = iron detritus

*Carbon*

$$\frac{\partial}{\partial t} DOC = \boldsymbol{\nabla} \bullet (K \boldsymbol{\nabla} DOC) - \frac{\partial}{\partial z} \boldsymbol{V} DOC + \Phi\, \delta \sum \mu_i P_i + \Phi\, \omega H + \lambda_D D_C - \varphi DOC \tag{A10}$$

$$\frac{\partial}{\partial t} DIC = \boldsymbol{\nabla} \bullet (K \boldsymbol{\nabla} DIC) - \frac{\partial}{\partial z} \boldsymbol{V} DIC - \Phi \sum \mu_i P_i + \Phi \Omega \sum \mu_i P_i + \Phi\, \Theta H + \varphi DOC + \frac{R\alpha_N D_C}{(C:N)}$$
$$+ AO_{CO_2} \tag{A11}$$

where the symbols and values are identified in Table 1. Bold denotes a vector quantity. All biological processes are assumed to cease in the presence of sea ice, in proportion to the fraction of sea ice cover, which is included as an external forcing field.

## 6.2 NASA Ocean Biogeochemical Model-Description

### *Circulation Model*

The Ocean General Circulation Model (OGCM) is a reduced gravity representation of circulation fields (Schopf and Loughe, 1995). It is global in scale, extending from near the South Pole to $72^o$ N, in increments of $2/3^o$ latitude and 1 1/4$^o$ longitude, comprising all regions where bottom depth > 200m. The model contains 14 vertical layers, in quasi-isopycnal coordinates, and is driven by wind stress, sea surface temperature, and shortwave radiation.

### *Radiative Model*

Radiative transfer calculations provide the underwater irradiance fields necessary to drive growth of the phytoplankton groups, and interact with the heat budget. The Ocean-Atmosphere Radiative Model (OARM; Gregg, 2002) contains a treatment of the spectral and directional properties of radiative transfer in the oceans, and explicitly accounts for clouds. The atmospheric radiative model is based on the Gregg and Carder (1990) spectral model, extended to the spectral regions 200 nm to 4 μm. It requires external monthly climatologies of cloud properties (cloud cover and liquid water path), surface pressure, wind speeds, relative humidity, precipitable water, and ozone. Aerosols are considered to be strictly of marine origin and are computed as in Gregg and Carder (1990).

Oceanic radiative properties are driven by water absorption and scattering, the optical properties of the phytoplankton groups, and chromophoric dissolved organic matter (CDOM). Three irradiance paths are enabled: a downwelling direct path, a downwelling diffuse (scattered)

path, and an upwelling diffuse path. All oceanic radiative calculations include the spectral nature of the irradiance.

Optical properties of coccolithophores and other phytoplankton groups were derived from laboratory studies. Their values and references can be found in Gregg (2002).

*Phytoplankton*

The growth formulation includes dependence on total irradiance ($E_T$), nitrogen as nitrate plus ammonium ($N_T$), silica (Si – for diatoms only), iron (Fe), and temperature (T)

$$\mu_i = (\mu_{max})_i \min[f(N_T, Si, Fe, E_T)_i] \, RG_i \tag{A12}$$

where i indicates the phytoplankton functional group index (in order, diatoms, chlorophytes, cyanobacteria, and coccolithophores), $\mu$ is the total specific growth rate ($d^{-1}$) of phytoplankton, $\mu_m$ is the maximum growth rate at $20^{\circ}C$ (Table 1). The term $\mu(E_T)$ represents the growth rate as a function solely of the total irradiance ($\mu$mol quanta $m^{-2} s^{-1}$),

$$f_i(E_T) = \frac{E_T}{(E_T + (k_E)_i)} \tag{A13}$$

where $k_E$ is the irradiance at which $\mu = 0.5\mu_m$ and equals $0.5 \, I_k$, where $I_k$ is the light saturation parameter. The nutrient-dependent growth terms are

$$f_i(NO_3) = \frac{NO_3}{(NO_3 + (k_N)_i)} \tag{A14}$$

$$f_i(NH_4) = \frac{NH_4}{(NH_4 + (k_N)_i)} \tag{A15}$$

$$f_i(N_T) = f_i(NH_4) + \min[f_i(NO_3), 1] - f_i(NH_4) \tag{A16}$$

(Gregg and Walsh, 1992)

$$f_i(Si) = \frac{Si}{[Si + (k_s)_i]} \tag{A17}$$

$$f_i(Fe) = \frac{Fe}{[Fe + (k_F)_i]} \tag{A18}$$

Temperature-dependent growth is from Eppley (1972)

$$R = 1.066^{(T-20^{\circ}C)} \tag{A19}$$

which produces a temperature-growth factor normalized to 20°C. The term G in Eq. A12 is an additional adjustment used for the cyanobacteria component that reduces their growth rate in cold water (<15°C)

$$G_3 = 0.0294T + 0.558 \qquad\qquad (A20)$$

$G_i = 1$ for the other three phytoplankton components (i=1,2,4) where 0.0294 is in units of per degree Celsius. When T≥15°C, $G_3$ reaches its maximum value of 1. This effect conforms to observations that cyanobacteria are scarce in cold waters (Agawin et al., 2000; 1998).

The cyanobacteria component possesses a modest ability to fix nitrogen from the water column, as observed in *Trichodesmium* spp. (Carpenter & Romans 1991). The nitrogen fixation is expressed as additional growth occurring when nitrogen availability is $<(k_N)_3$,

$$\mu_{nfix} = 0.25 \exp(-75P_3) \qquad\qquad (A21)$$

where the index 3 indicates cyanobacteria. The biomass dependence represents a progressive community changeover from non-N-fixing cyanobacteria to N-fixing bacteria as the total population declines under nitrogen-stressed conditions. The total N-limited growth rate plus the additional growth derived from N-fixation is not allowed to exceed the growth rate where total nitrogen = $(k_N)_3$. No accounting for denitrification is made in the model.

Photoadaptation is simulated by stipulating 3 states: 50, 150 and 200 (μmol quanta m$^{-2}$ s$^{-1}$). This is based on laboratory studies which typically divided experiments into low, medium, and high classes of light adaptation. Carbon:chlorophyll ratios (Φ) are kept constant at 50 g:g for mass conservation.

Mean irradiance is computed during daylight hours, and then the phytoplankton photoadaptive state is classified accordingly. This calculation is only performed once per day to simulate a delayed photoadaptation response. Light saturation constants for the three light levels are provided in Table 1.

Phytoplankton group physiological parameters $\mu_m$, $I_k$, and $k_{N,S,F}$ are derived from carefully controlled, inter-comparative laboratory studies. We require that at least two of the groups are involved simultaneously in order to utilize the experimental results. For $\mu_m$ mean values of the relative growth rates are derived from the results of Ben-Amotz and Gilboa (1980), Brand et al. (1986, 1983), Eppley et al. (1969), Falkowski et al. (1985), Furnas (1991), Gavis et al. (1981), Goldman and Glibert (1982), Humphrey (1979), Subba Rao (1981), and Sunda and Huntsman (1995).

Light saturation parameters, $I_k$, are formulated for the three irradiance categories used to define photoadaptation. Mean values are summarized from the reports of Barlow and Alberte (1985), Bates and Platt (1984), Langdon (1987), Perry et al. (1981), Sakshaug and Andresen (1986), and Wyman and Fay (1986).

The coccolithophore half-saturation constant for nitrogen ($k_N$) was observed by Eppley (1969) to be one-half the value of diatoms. Cyanobacteria $k_N$ is set slightly lower than

coccolithophores, assuming small particle size leads to improved nutrient uptake efficiency. Chlorophyte $k_N$ is set at one-third the departure between diatoms and coccolithophores. The diatom $k_N$ is arbitrarily set to 1 μM.

Phytoplankton vector sinking is treated as additional advection in the z-direction. Sinking rates are specified at 31$^\circ$C and derived from Stokes Law using representative phytoplankton sizes from Ahn et al. (1992), Bricaud and Morel (1986), Bricaud et al. (1983; 1988), Dubinsky and Berman (1986), Kirk (1980); Mitchell and Kiefer (1988), Morel (1987), Morel and Bricaud (1981), and Sathyendranath et al. (1987), for the individual groups. The rates are adjusted by viscosity according to Stokes Law (Csanady, 1986), which is parameterized here by temperature

$$w_s(T) = w_s(31°C)[0.451 + 0.0178T] \qquad (A22)$$

Coccolithophore sinking rates are allowed to vary as a function of growth rate from 0.3 to 1.4 m d$^{-1}$ based on observations by Fritz and Balch (1996). A linear relationship is assumed

$$w_{s4} = 0.752\mu_4(high) + 0.225 \qquad (A23)$$

where $w_s$ is the sinking rate of coccolithophores (m d$^{-1}$), $\mu$(high) is the highest growth rate actually achieved for the previous day, and the subscript 4 represents coccolithophores.

### *Nutrients*

The diversity in the processes affecting the four nutrient groups requires elucidation in 4 separate equations, unlike the phytoplankton. All are taken up by phytoplankton growth, with silica subject only to diatom uptake (note the subscript=1 in Eq. A4 denoting diatoms). For three of the nutrients, nitrate, silica, and dissolved iron, corresponding detrital pools remineralize to return nutrients previously uptaken by phytoplankton. There is no detrital pool for ammonium, which is excreted as a function of herbivore grazing, and as a function of higher order ingestion of herbivores, represented by the term $n_2H^2$ in Eqs. A3, A5, A6, A7, and A9. Dissolved iron also has an excretion pathway, but nitrate and silica do not. The nutrient to chlorophyll ratios, denoted b in Eqs. A2-A5, are derived from Redfield ratios (Table 1) and the carbon:chlorophyll ($\Phi$) ratio is constant.

$$b_N = \Phi/C{:}N \qquad (A24)$$
$$b_S = \Phi/C{:}S \qquad (A25)$$
$$b_F = \Phi/C{:}Fe \qquad (A26)$$

As in Gregg et al. (2003) dust deposition fields are derived from Ginoux et al. (2001). In this model, four dust size fractions are transported, corresponding to clay (smallest) and three increasing fractions of silt. The iron content is assumed to vary among the clay and silt fractions as follows: clay = 3.5% iron, silt = 1.2% iron (Fung et al., 2000). Iron solubility is assumed at 2% for all fractions, which is toward the low end of current estimates (Fung et al., 2000), but is the same as used by Moore et al. (2004). The bottom boundary condition is 0.6 nM (Archer and Johnson, 2000)

Iron scavenging is implemented in this version of NOBM. It is set at 2.74x10$^{-5}$ d$^{-1}$ at low iron concentrations (<0.6nM; Moore et al., 2002) and 50 times this rate at higher concentrations. A smooth transition is enabled as in Moore et al. (2002)

$$\theta = 2.74 \times 10^{-5} N_F, for\ N_F < 0.6 nM \tag{A27}$$
$$\theta = 2.74 \times 10^{-5} N_F + 1.37 \times 10^{-3}(N_F - 0.6), for\ N_F \geq 0.6 nM \tag{A28}$$

*Herbivores*

Grazing uses an Ivlev formulation (McGillicuddy et al., 1995),

$$\gamma(T) = \gamma_m R_H [1 - \exp(-\Lambda \Sigma_i P_i)] \tag{A29}$$

$R_H$ is the maximum grazing rate at 20$^o$ C ($\gamma_m$) adjusted by temperature

$$R_H = 0.06 \exp(0.1T) + 0.70 \tag{A30}$$

The temperature-dependence for grazing is more linear than that for phytoplankton, reflecting the larger size of their overall community. The grazing represents the total loss of phytoplankton to herbivores, as indicated by the summation symbol, but is applied to the individual phytoplankton functional groups proportionately to their relative abundances. This enables herbivore grazing to self-adapt the prevailing phytoplankton community.

The two loss terms in Eq. A6 represent the death of herbivores ($\eta_1 H$) and higher order heterotrophic losses ($\eta_2 H^2$). These formulations and parameters (Table 1) were taken from McGillicuddy et al. (1995).

*Detritus*

Three detrital components represent the three major nutrient elements, carbon/nitrogen, silica, and iron (Eq. A6-A9). The nitrogen detritus is kept as carbon in the model, but since the C:N ratio is constant, it is simple to convert when needed. All are subject to advection, diffusion and sinking. Detrital sinking, like phytoplankton sinking, is dependent on viscosity parameterized here in terms of temperature, using the same formulation. Remineralization, $\kappa$, is also temperature-dependent, and uses the phytoplankton growth-dependence term R in Eq. A19. Silica contained in the diatom component of phytoplankton is assumed to pass through herbivores upon grazing directly into the silica detritus pool. No silica remains in the herbivore component at any time.

*Carbon*

Dissolved organic carbon cycling is taken from Aumont et al. (2002), with conversions added for compatibility with NOBM units. In addition, all parameters are temperature-dependent,

unlike Aumont et al. (2002), using the phytoplankton temperature dependence defined in Eq. A19. Following Aumont et al. (2002), excretion of DOC by the herbivore component is

$$\omega = r_H \frac{H}{H_0 + H} \, R \qquad (A31)$$

where $r_H$ is the herbivore excretion rate at $20^o$C, and $H_o$ is the half-saturation constant for excretion (Table 1). $H_o$ is adjusted from units of $\mu$M carbon in Aumont et al. (2002) to mg m$^{-3}$ chlorophyll to conform to the NOBM units for herbivores. Bacterial degradation of DOC is represented by

$$\varphi = \lambda_{DOC} \frac{N_1}{K_1 + N_1} \frac{DOC}{K_2 + DOC} \, DOC \, R \qquad (A32)$$

where $\lambda_{DOC}$ is the DOC remineralization rate and $K_1$ and $K_2$ are half-saturation constants for remineralization (Aumont et al., 2002; Table 1). Aumont et al. (2002) used phosphate, so here we substitute nitrate, since phosphate is not available in NOBM. Again parameters are allowed to vary as a function of temperature. In addition, the value for $K_1$ was increased by a factor of 10 to convert to nitrate rather than phosphate. According to Conkright et al. (1994), nitrate contours generally follow phosphate but nitrate concentrations are approximately 10 times higher.

Dissolved inorganic carbon has a single sink, uptake by phytoplankton during photosynthesis, and sources deriving from respiration by phytoplankton $\Omega$ in the process of growth, herbivores $\Theta$ at all times, and bacteria $\varphi$ in the process of degrading DOC. There is also an interaction with the atmosphere ($AO_{CO2}$) which can be a source or a sink depending upon the difference in partial pressures of $CO_2$ in the ocean and atmosphere ($\Delta pCO_2$), and the ability for gas to transfer across the ocean surface interface. These complex processes are follow procedures described by the Ocean Carbon Model Intercomparison Project (Dutay et al., 2002; Doney et al., 2004; http://www.ipsl.jussieu.fr/OCMIP/).

Table 1. Notation, parameters, and variables for NOBM. Values are provided for the parameters and ranges are provided for the variables. When a parameter varies according to temperature, the value at a specified temperature is shown and identified. Nutrient/chlorophyll ratios are variable because of photadaptation-dependence, and only the range is shown, corresponding to low-, and high-light adaptation, and therefore also corresponding to C:chlorophyll ratios of 20 to 80 g g$^{-1}$. All time units are converted to s$^{-1}$ before use in A(1) to A(11).

| Symbol | Parameter/Variable | | | Value | Units |
|---|---|---|---|---|---|
| *General* | | | | | |
| K | Diffusivity | | | Variable | m$^2$ s$^{-1}$ |
| ∇ | 3D Gradient operator | | | none | none |
| **V** | 3D Vector velocity | | | Variable | m s$^{-1}$ |
| L | Layer thickness | | | Variable | m |
| | | | | | |
| *Phytoplankton* | | | | | |
| $w_s$ | Sinking rate of phytoplankton at 31°C | | | | |
| | Diatoms | | | 0.75 | m d$^{-1}$ |
| | Chlorophytes | | | 0.25 | m d$^{-1}$ |
| | Cyanobacteria | | | 0.0085 | m d$^{-1}$ |
| | Coccolithophores | | | 0.3-1.4 | m d$^{-1}$ |
| μ | Specific growth rate of phytoplankton maximum ($μ_m$) at 20°C: | | | | |
| | Diatoms | | | 2.00 | d$^{-1}$ |
| | Chlorophytes | | | 1.68 | d$^{-1}$ |
| | Cyanobacteria | | | 1.33 | d$^{-1}$ |
| | Coccolithophores | | | 1.50 | d$^{-1}$ |
| κ | Senescence rate | | | 0.05 | d$^{-1}$ |
| $k_E$ | Half-saturation for growth as function of quota | | | $0.5I_k$ | μmol quanta m$^{-2}$ s$^{-1}$ |
| $E_T$ | Total quanta (direct+diffuse) | | | variable | μmol quanta m$^{-2}$ s$^{-1}$ |
| R | Temperature dependence for growth | | | 0.25-9.4 | none |
| G | Temperature-dependence for cyanobacteria growth | | | 0.5-1.0 | none |
| $I_k$ | Light Saturation | | | | |
| | Light level: | Low (50) | Medium (150) | High (200) | |
| | diatoms | 90.0 | 93.0 | 184.0 | μmol quanta m$^{-2}$ s$^{-1}$ |
| | chlorophytes | 96.9 | 87.0 | 143.7 | μmol quanta m$^{-2}$ s$^{-1}$ |
| | cyanobacteria | 65.1 | 66.0 | 47.0 | μmol quanta m$^{-2}$ s$^{-1}$ |
| | coccolithophore | 56.1 | 71.2 | 165.4 | μmol quanta m$^{-2}$ s$^{-1}$ |
| *Nutrients (N)* | | | | | |
| $b_{N,S,F}$ | Nutrient:chlorophyll ratio | | | | |
| | Nitrogen | | | 0.63 | μM (μg l$^{-1}$)$^{-1}$ |
| | Silica | | | 1.26 | μM (μg l$^{-1}$)$^{-1}$ |
| | iron | | | 0.03 | μM (μg l$^{-1}$)$^{-1}$ |
| ε | Nutrient excretion | | | | |
| | Nitrate | | | 0.0 | d$^{-1}$ |
| | Ammonium | | | 0.10 | d$^{-1}$ |
| | Silica | | | 0.0 | d$^{-1}$ |
| | Iron | | | 0.10 | d$^{-1}$ |

| | | | |
|---|---|---|---|
| $k_N$ | Half-saturation constant nitrogen/carbon | | |
| | Diatoms | 1.0 | μM |
| | Chlorophytes | 0.67 | μM |
| | Cyanobacteria | 0.45 | μM |
| | Coccolithophores | 0.50 | μM |
| $K_S$ | Half-saturation constant silica | | |
| | Diatoms | 0.2 | μM |
| $K_F$ | Half-saturation constant iron | | |
| | Diatoms | 0.12 | nM |
| | Chlorophytes | 0.09 | nM |
| | Cyanobacteria | 0.08 | nM |
| | coccolithophores | 0.08 | nM |
| θ | Iron scavenging rate | | |
| | Low iron (<0.06nM) | $2.74 \times 10^{-5}$ | $d^{-1}$ |
| | High iron ($\geq 0.06$nM) | $1.37 \times 10^{-3}$ | $d^{-1}$ |
| $A_{Fe}$ | Atmospheric deposition of iron | 0.03-967.0 | nmol $m^{-2}$ $d^{-1}$ |
| C:N | Carbon:nitrogen ratio | 79.5 | μg $l^{-1}$ $(μM)^{-1}$ |
| C:S | Carbon:silica ratio | 79.5 | μg $l^{-1}$ $(μM)^{-1}$ |
| C:Fe | Carbon:iron ratio | 1800 | μg $l^{-1}$ $(nM)^{-1}$ |
| *Herbivores (H)* | | | |
| γ | Grazing rate maximum ($\gamma_m$) at 20°C | 1.2 | $d^{-1}$ |
| Λ | Ivlev constant | 1.0 | $(μg\ l^{-1})^{-1}$ |
| $\eta_1, \eta_2$ | Heterotrophic loss rates | 0.1,0.5 | $d^{-1}$ |
| $R_H$ | Temperature-dependence for grazing | 0.75-2.7 | none |
| *Detritus (D)* | | | |
| $w_d$ | Sinking rate of detritus at 31°C | | |
| | Carbon/nitrogen detritus | 40.0 | m $d^{-1}$ |
| | Silica detritus | 50.0 | m $d^{-1}$ |
| | Iron detritus | 5.0 | m $d^{-1}$ |
| $\alpha_{C,S,F}$ | Remineralization rate at 20°C | | |
| | Carbon/nitrate | 0.01 | $d^{-1}$ |
| | Silica | 0.05 | $d^{-1}$ |
| | iron | 0.50 | $d^{-1}$ |
| Φ | Carbon:chlorophyll ratio | Variable | g $g^{-1}$ |
| *Carbon (DOC, DIC)* | | | |
| δ | Phytoplankton DOC exudation fraction | 0.05 | none |
| $r_H$ | Excretion rate of DOC by herbivores at 20°C | 0.05 | $d^{-1}$ |
| $H_o$ | Half-saturation constant for herbivore excretion of DOC | 0.14 | mg $m^{-3}$ |
| $\lambda_D$ | Detrital breakdown rate at 20°C | 0.05 | $d^{-1}$ |
| $\lambda_{DOC}$ | Remineralization rate of DOC to nitrate | 0.005 | $d^{-1}$ |
| ω | Herbivore excretion function for DOC | variable | $d^{-1}$ |
| Ω | Phytoplankton respiration fraction | 0.05 | none |
| Θ | Herbivore respiration | 0.05 | $d^{-1}$ |

| Φ | Bacterial degradation of DOC to DIC | variable | $d^{-1}$ |
|---|---|---|---|
| $K_1$ | First half-saturation constant for remineralization to nitrate | 3.0 | $\mu M$ |
| $K_2$ | Second half-saturation constant for remineralization to nitrate | 15.0 | $\mu M$ |
| $AO_{CO2}$ | Atmospheric-oceanic $CO_2$ Equilibration | Variable | $\mu atm$ |

# 7　Appendix B: Acknowledgements

# Previous Volumes in This Series

**Volume 1**
*September 1994*

Documentation of the Goddard Earth Observing System (GEOS) general circulation model - Version 1
**L.L. Takacs, A. Molod, and T. Wang**

**Volume 2**
*October 1994*

Direct solution of the implicit formulation of fourth order horizontal diffusion for gridpoint models on the sphere
**Y. Li, S. Moorthi, and J.R. Bates**

**Volume 3**
*December 1994*

An efficient thermal infrared radiation parameterization for use in general circulation models
**M.-D. Chou and M.J. Suarez**

**Volume 4**
*January 1995*

Documentation of the Goddard Earth Observing System (GEOS) Data Assimilation System - Version 1
**James Pfaendtner, Stephen Bloom, David Lamich, Michael Seablom, Meta Sienkiewicz, James Stobie, and Arlindo da Silva**

**Volume 5**
*April 1995*

Documentation of the Aries-GEOS dynamical core: Version 2
**Max J. Suarez and Lawrence L. Takacs**

**Volume 6**
*April 1995*

A Multiyear Assimilation with the GEOS-1 System: Overview and Results
**Siegfried Schubert, Chung-Kyu Park, Chung-Yu Wu, Wayne Higgins, Yelena Kondratyeva, Andrea Molod, Lawrence Takacs, Michael Seablom, and Richard Rood**

**Volume 7**
*September 1995*

Proceedings of the Workshop on the GEOS-1 Five-Year Assimilation
**Siegfried D. Schubert and Richard B. Rood**

**Volume 8**
*March 1996*

Documentation of the Tangent Linear Model and Its Adjoint of the Adiabatic Version of the NASA GEOS-1 C-Grid GCM: Version 5.2
**Weiyu Yang and I. Michael Navon**

**Volume 9**
*March 1996*

Energy and Water Balance Calculations in the Mosaic LSM
**Randal D. Koster and Max J. Suarez**

**Volume 10**
*April 1996*

Dynamical Aspects of Climate Simulations Using the GEOS General Circulation Model
**Lawrence L. Takacs and Max J. Suarez**

**Volume 11**
*May 1997*

Documentation of the Tangent Linear and its Adjoint Models of the Relaxed Arakawa-Schubert Moisture Parameterization Package of the NASA GEOS-1 GCM (Version 5.2)
**Weiyu Yang, I. Michael Navon, and Ricardo Todling**

**Volume 12**
*August 1997*

Comparison of Satellite Global Rainfall Algorithms
**Alfred T.C. Chang and Long S. Chiu**

**Volume 13**
*December 1997*

Interannual Variability and Potential Predictability in Reanalysis Products
**Wie Ming and Siegfried D. Schubert**